

**Chaotic renormalization flow in the Potts model induced by long-range competition**Kejin Jiang <sup>1</sup>, Jianyong Qiao <sup>1,\*</sup> and Yueheng Lan <sup>1,2,†</sup><sup>1</sup>*School of Science, Beijing University of Posts and Telecommunications, Beijing 100876, China*<sup>2</sup>*State Key Lab of Information Photonics and Optical Communications, Beijing University of Posts and Telecommunications, Beijing 100876, China*

(Received 4 January 2021; accepted 19 May 2021; published 14 June 2021)

A proper description of spin glass remains a hard subject in theoretical physics and is considered to be closely related to the emergence of chaos in the renormalization group (RG) flow. Previous efforts concentrate on models with either complicated or nonrealistic interactions in order to achieve this chaotic behavior. Here we find that the commonly used Potts model with long-range interaction could do the job nicely in a large parameter regime as long as the competition between the ferromagnetic and antiferromagnetic interaction is maintained. With this simplicity, the appearance of chaos is observed to sensitively depend on the detailed network structure: the parity of bond number in a branch of the basic RG substituting unit; chaos only emerges for even numbers of bonds. These surprising and universal findings may shed light on the study of spin glass.

DOI: [10.1103/PhysRevE.103.062117](https://doi.org/10.1103/PhysRevE.103.062117)**I. INTRODUCTION**

In the paper “Statistical theory of equations of state and phase transitions,” Yang and Lee mentioned that the problem of phase transitions and equation of state is closely related to the distribution of roots of the grand partition function [1,2]. For a large class of problems of practical interest, the roots behave remarkably well. For example, these zeros for an Ising ferromagnet lie on the unit circle when exposed to a magnetic field [1–3]. For a system with finite size, there is no real root but the set of zeros may approach a specific point on the real axis in the thermodynamic limit which indicates a phase transition at the point. In fact, the type of the phase transition can be deduced from the distribution of zeros near the positive real axis [4]. So, an accurate determination of the grand partition function is essential for the study of phase transition.

Unfortunately, very few models can be solved exactly in statistical physics. However, the invention of the renormalization group (RG) technique provides a powerful tool for this type of computation and greatly advances our understanding of phase transitions [5–7]. The RG theory investigates change of physical laws across scales by defining a flow or a map relating parameters at different scales. Phase transition is determined by the critical manifold of a certain fixed point of the RG flow in the parameter space, which is closely related to scale invariance or self-similarity [8,9].

On the other hand, the partition function could be evaluated in an iterative way. With one renormalization parameter, the support of Yang-Lee zeros is the Julia set of the RG map in the thermodynamic limit [8,10–13]. In this way, the problem of finding distribution of roots converts to the study of the Julia

set of the RG map in the complex plane [8,12]. For bulk materials, the dynamics of the RG map is simple on the real axis, consisting of several basins of attraction of stable fixed points separated by unstable ones [14], which serve to distinguish different phases. As an example, the phase transition point of the well-known Ising model [15,16] could be accurately located with the real-space RG [17].

Nevertheless, in special circumstances, the RG dynamics could be periodic or even chaotic [11–13,18,19]. In the complex plane, chaotic RG trajectories are not so rare [20–23]. Interestingly, these types of trajectories are also found in the study of spin glass [24–28], which is a very special condensed matter state and characterized by disorder and frustration [29,30] but displays cooperative behavior in a non-conventional way [31]. Approximate or exact RG flows are constructed for models with random coupling and for spins on hierarchical lattices but with quite unphysical or artificial couplings interactions [20,22,23,32–35]. It is also found that the multiplicity in spin states could oust chaos [36]. These models provide interesting pictures for the spin glass transition.

In literature, many spin systems sitting on hierarchical lattices could be exactly solved by the RG, among which stands the Potts model [8,21,37,38]. It is a generalization of the famous Ising model but the number of states of each spin goes beyond two [13,39]. Very often, the derived exact RG map [40,41] has a Julia set more complex than a unit circle since the required condition for the Lee-Yang circle theorem is not satisfied any longer. Nevertheless, on the real axis, the dynamics seems always simple. In a recent paper [38], unexpectedly Qiao found that on a diamond hierarchical lattice at some particular parameter values the Julia set of the RG map of the Potts model fills densely a closed segment of the real axis with its dynamics being chaotic [38,42,43]. Nevertheless, for this to happen, the number of spin states at each site is not an integer any more, which does not seem to make much physical sense. A natural question is whether this

\*Corresponding author: [qjy@bupt.edu.cn](mailto:qjy@bupt.edu.cn)†Corresponding author: [lanyh@bupt.edu.cn](mailto:lanyh@bupt.edu.cn)

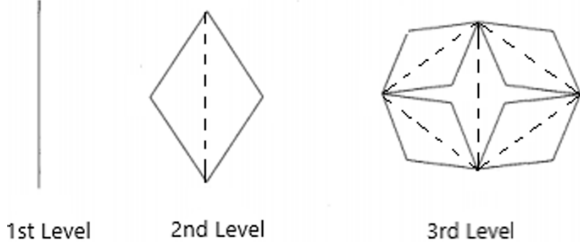


FIG. 1. First three levels of the hierarchical diamond lattice model for  $m = n = 2$ . The solid lines denote the structure at the current level and the dashed lines mark all previous connections.

observation could be made in a more general context which might be physically relevant.

In this paper, we found that if antiferromagnetic long-range interactions are properly supplied to compete with the ferromagnetic ones, the chaotic RG map becomes a frequent occurrence. If this competition could be reconciled with no presence of frustration, chaos will not appear as surprisingly demonstrated with a very small variation of the network structure: the bond number changing from even to odd integers in each branch of the basic RG block. Our findings may shed light on the study of statistical properties of complex systems with hierarchical structures.

## II. POTTS MODEL ON A HIERARCHICAL DIAMOND LATTICE

A hierarchical lattice [44] could be constructed by iteration. We start with two nodes (two spins) connected with a bond (first level), which stands for a direct interaction. The basic construction step is to replace each bond with a diamondlike structure containing  $m$  branches each of which has  $n$  consecutive bonds (second level), together with  $m(n - 1)$  new spins, sitting on the joints of the bonds. To proceed to the next level, each bond of the current level is replaced again by the above diamondlike structure. In Fig. 1, the first three levels of the hierarchical diamond lattice are plotted with solid lines in which  $m = n = 2$ .

The structure is self-similar and each spin has  $\lambda$  states [45], constituting the Potts model in which  $\lambda = 2$  recovers the Ising model. The Hamiltonian without external magnetic field can be written as

$$H = -J \sum_{\langle i, j \rangle} \delta(s_i, s_j), \quad (1)$$

where  $s_i, s_j$  are two spin states and  $\langle i, j \rangle$  represents all the nearest neighboring spin pairs.  $J$  is the coupling constant with  $J > 0$  ( $J < 0$ ) indicating the (anti)ferromagnetic interaction and  $\delta(s_i, s_j)$  is the Kronecker delta function which is one when the two arguments are equal and zero otherwise.

To get statistical properties of the system, we need to compute the partition function, which at the  $p$ th level is given by

$$Z_p = \sum_{\{s_i\}} \exp \left[ K \sum_{\langle i, j \rangle} \delta(s_i, s_j) \right], \quad (2)$$

where  $K = \frac{J}{k_B T}$ , with  $k_B$  and  $T$  being the Boltzmann constant and the temperature, respectively. The outer summation is over all the spin configurations. For later convenience, we employ the convention  $e^K = z$ . By invoking the RG transformation [38] (also see Appendix A), we get the recursion relation for the partition function  $Z_j$  between neighboring levels

$$Z_j(z) = f_{mn\lambda, j}(z) Z_{j-1}(\omega), \quad (3)$$

where

$$\omega = U_{mn\lambda}(z) = \left[ \frac{(z + \lambda - 1)^n + (\lambda - 1)(z - 1)^n}{(z + \lambda - 1)^n - (z - 1)^n} \right]^m \quad (4)$$

defines the RG map and

$$f_{mn\lambda, j}(z) = \left[ \frac{(z + \lambda - 1)^n - (z - 1)^n}{\lambda} \right]^{m^{j-1} n^{j-2}} \quad (5)$$

is the integrated-out part. Through repeated application of Eqs. (3) and (4), the partition function of the hierarchical lattice could be obtained up to any level.

It has been shown that the set of Lee-Yang zeros in the thermodynamic limit coincides with the Julia set of the RG map [8, 13, 44]. In most cases, the Julia set meets the real axis at discrete points but for  $m = 2$ ,  $n = 5$ , and  $\lambda \approx 1.824$ , unexpectedly, the intersection of the Julia set with the real axis contains a closed interval lying in  $(-0.02, 0.2)$  [38], with the dynamics being chaotic, which seems very surprising, considering the simplicity of the Hamiltonian Eq. (1) that contains no competing interactions and the regular lattice structure.

Nevertheless, as  $\lambda$  represents the number of spin states in the Potts model, it should be an integer in a real physical system. But it is proved that, for integer values of  $\lambda$ , no chaotic behavior could be found on the real axis. What is needed to maintain chaos in the RG map for more realistic parameters?

## III. CHAOTIC RENORMALIZATION FLOW WITH LONG-RANGE INTERACTION

Interestingly, we find that in the thermodynamic limit, adding long-range antiferromagnetic interaction will produce chaotic RG trajectories in a wide range of parameter values. Specifically, when carrying out the RG transformation, instead of removing the original link and replacing it with four new links, we keep the original link but assign a different interaction, which is marked as a dashed line in Fig. 1.

Of course the four new links are still supplied, which are marked with solid lines. In the ensuing steps, only the solid lines are expanded. Physically, the dashed lines stand for long-range interaction. A similar setup could be found in the literature [46] but with a very artificial interaction strength. Below, we will show that, with constant or even decaying interaction, the RG trajectories could keep chaotic. The partition function of the new model is shown as

$$Z = \sum_{s_i} \exp \left[ K \sum_{\langle i, j \rangle} \delta(s_i, s_j) + (-\beta') \sum_{\text{dashed line}} \delta(s_i, s_j) \right], \quad (6)$$

where  $(-\beta')$  indicates the coupling constant of the new antiferromagnetic interaction and the related summation is over all the spin pairs connected by a *dashed line*.

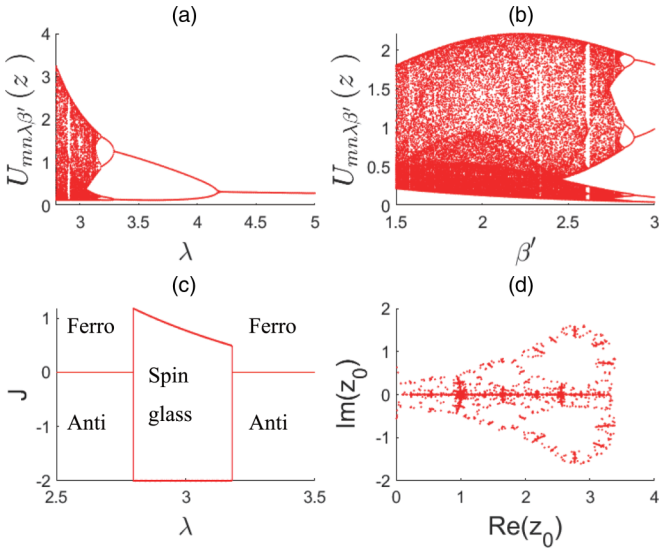


FIG. 2. Bifurcation diagram for the RG map  $U_{mn\lambda\beta'}(z)$  [Eq. (7)] on the real axis (a) at  $m = 6, n = 2$ , and  $\beta' = 2$ , with respect to  $\lambda$ , and (b) with respect to  $\beta'$ , at  $m = 6, n = 2$ , and  $\lambda = 3$ , and the phase diagram (c) deduced from (a) in the  $\lambda - J$  plane and the associated Julia set in the complex plane (d) for  $\lambda = 3$ .

For this new model, a similar RG calculation (see Appendix B) gives the exact RG map  $U_{mn\lambda\beta'}(z)$ ,

$$U_{mn\lambda\beta'}(z) = e^{-\beta'} \left[ \frac{(z + \lambda - 1)^n + (\lambda - 1)(z - 1)^n}{(z + \lambda - 1)^n - (z - 1)^n} \right]^m, \quad (7)$$

where the factor  $e^{-\beta'}$  accounts for the influence of the long-range interaction.

For  $\lambda \in [1, 6]$ ,  $m = 6, n = 2$ , and  $\beta' = 2$ , on the real axis, the bifurcation diagram of the above RG map is shown in Fig. 2(a), where we iterate the map  $U_{mn\lambda}(z)$  500 times, and plot the last 200 points.

In Fig. 2(a), the empty space (not shown) at  $\lambda \in [2.5, 2.80]$  indicates the fact that, in this range, the RG iteration tends to infinity eventually so that there is no finite point on the real axis that can be recorded and plotted. With a decrease of  $\lambda$ , the bifurcation diagram clearly shows a period doubling route to chaos and the alternating periodic windows. Especially, at  $\lambda = 3$ , the system seems chaotic, which may be of physical significance. The onset of chaos starts at  $\lambda \approx 3.18$ , and a periodic-2 orbit appears at  $\lambda \approx 3.29$ . When  $\lambda \approx 4.225$ , the RG map reaches a globally stable fixed point. It is easy to check that, with the introduction of the long-range interaction, chaotic trajectories on the real axis may appear also in many other cases. For example, at  $\beta' \in [1, 3.9]$ ,  $m = 6, n = 2, \lambda = 3$ , the bifurcation diagram is shown in Fig. 2(b). In some papers [24,36], similar behavior could be observed but only with infinitely strong antiferromagnetic interaction, which seems unphysical. In Fig. 2(d), the Julia set of the RG map Eq. (7) is displayed at  $m = 6, n = 2, \lambda = 3$ , and  $\beta' = 2$ , which is symmetric and intersects the real axis in a considerable range, indicating large variations of the effective coupling strength.

The maximum Lyapunov exponent  $\eta$  is often used to characterize the chaotic dynamics [47], which could here be

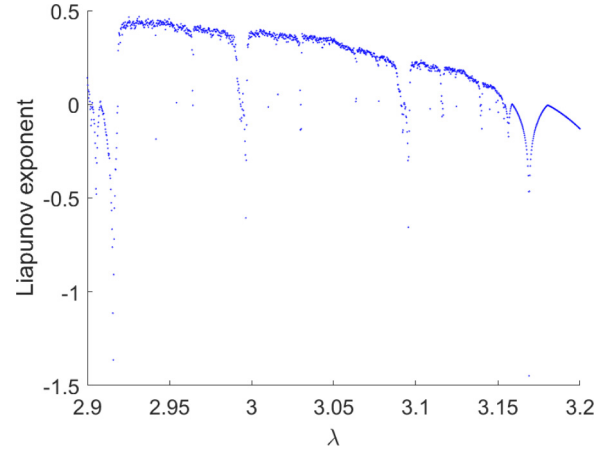


FIG. 3. Lyapunov exponent of  $U_{mn\lambda\beta'}(z)$  [Eq. (7)] at  $m = 6, n = 2$ , and  $\beta' = 2$ , with  $\lambda \in [2.9, 3.2]$ .

computed as

$$\eta = \lim_{j \rightarrow \infty} \left\{ \frac{1}{j} \sum_{i=0}^{j-1} \ln \left| \frac{\partial U_{mn\lambda\beta'}(z_i)}{\partial z_i} \right| \right\}, \quad (8)$$

where  $j$  is the number of iteration steps. We choose a part of the chaotic region in Fig. 2(b) to calculate  $\eta$  and plot the result in Fig. 3, where the computation is carried out with  $\lambda \in [2.9, 3.2]$ .

It can be seen from Fig. 3 that, except for a few small windows,  $\eta$  is bigger than zero. Especially, at  $\lambda = 3, \eta = 0.366$ , indicating that the map is indeed chaotic. The set of points in which  $\eta < 0$  signals the emergence of periodic windows. In the above investigation,  $\lambda$  is chosen to be an integer on purpose for possible physical realization.

In fact, the chaotic RG trajectory emerges quite often in the situation with long-range interaction. As shown in Table I, Lyapunov exponents are all greater than zero with different integer values of  $\lambda$ . In literature, chaos in the RG trajectory is often associated with spin glass [24]. Spin glass is a special material state which has unusual properties and is characterized with complex energy landscape [48]. Below the critical freezing temperature, the ergodicity is broken such that the state is lingering around some local energy minimum. Viewed locally, each patch of the whole spin network resides possibly in a different configuration and the dominant ones depend sensitively on temperature or external fields [49]. This sensitive dependence is generally regarded a salient feature of chaos [47] and could be observed as well in the RG transformation [24,50].

TABLE I. Lyapunov exponent  $\eta$  of the chaotic RG trajectories of  $U_{mn\lambda\beta'}(z)$  [Eq. (7)] at different parameters.

$m$	$n$	$\beta'$	$\lambda$	$\eta$
3	2	2	2	0.637
6	2	2	3	0.366
9	2	2	4	0.091
13	2	2	5	0.427
16	2	2	6	0.365

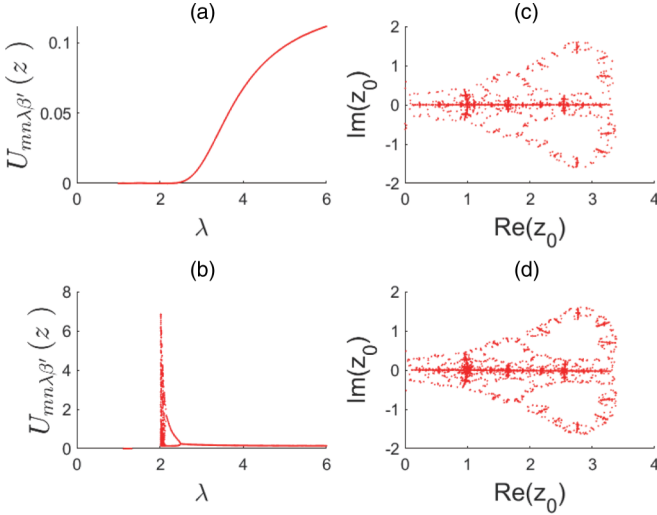


FIG. 4. Bifurcation diagram for the RG map  $U_{mn\lambda\beta'}(z)$  on the real axis at  $m = 6$ ,  $\beta' = 2$ , with respect to  $\lambda$ ,  $n = 3$  (a) and  $n = 4$  (b). The Julia set (nonwandering set within 30 steps) of the RG map when  $\beta'$  changes as  $CP^{-\alpha}$  (c) and as  $Ce^{-\alpha P}$  (d) at  $C = 2$ ,  $\alpha = 0.01$ ,  $\lambda = 3$ ,  $m = 6$ , and  $n = 2$ .

The parameter  $K = \frac{J}{k_B T}$  is a rescaled form of the interaction  $J$ . If we take  $k_B T = 1$ ,  $K = J$ . When  $K > 0$ ,  $J > 0$ , and  $z = e^K > 1$ , the interaction of spins is ferromagnetic. When  $K < 0$ ,  $J < 0$ , and  $0 < z = e^K < 1$ , the interaction is antiferromagnetic. Similarly, when  $\beta' > 0$ , the long-range interaction is antiferromagnetic and vice versa for  $\beta' < 0$ . The Julia set extends over the interval  $[0.1, 3.3]$  as displayed in Fig. 2(d), which indicates that the effective coupling constant  $K$  can be positive or negative at different levels of the network model. As we checked, chaotic RG trajectories do not appear for  $\beta' < 0$ , which articulates the importance of the competition between the two opposite types of interactions, a source for the generation of randomness and frustration as in spin glass [51]. Chaos will not appear if the absolute value of  $\beta'$  is too small since the ferromagnetic interaction then dominates. From the above calculation, a phase diagram is obtained as shown in Fig. 2(c). It is easy to see that, if  $\lambda$  is too big or too small, the glass phase vanishes and we have either ferromagnetic or antiferromagnetic phase. In this sense, the spin glass phase appears also out of a kind of quite subtle balance or competition between two opposite forces [52].

#### A. Parity of $n$ matters a lot

The bifurcation diagram with respect to  $\lambda$  for Eq. (7) is plotted with different  $n$ 's in Fig. 4. It is surprising that in this figure, when  $n$  is even, the map could reach chaos, while for odd  $n$  the map is never chaotic but arrives and stays at a stable fixed point. We also checked a sequence of other  $n$  values and found the same fact, which may be explained as follows. We know that  $n$  is the number of bonds in each branch of the basic substituting unit. When  $n$  is odd, if the renormalized coupling constant is negative, the paths through the solid and the dashed lines in Fig. 1 will be consistent with each other, being antiferromagnetic. There would be no frustration and a simple fixed point of the RG map representing the free energy

minimum could be achieved. In Fig. 4(a) for  $n = 3$ , we see that the stable fixed point  $z < 1$ , indicating  $J < 0$ , which is the case also for  $n = 5, 7, 9, \dots$ . However, when  $n$  is even as in Fig. 4(b), the overall effect of the  $m$  paths through the solid lines connecting the two end spins is always ferromagnetic, which competes with the antiferromagnetic interaction represented by the dashed line. So, in this case, the frustration is always present, which possibly leads to chaos and thus the sensitive dependence of the dominant configurations on the bond strength or temperature, as in all models of spin glass [48]. Without frustration as for an odd  $n$ , the spin glass phase never shows up in the present context. We also checked the bifurcation diagram for different  $m$ 's but found no obvious connection to the chaotic behavior.

#### B. RG flow with decaying interaction

The RG relates physical laws across different scales. The more the iteration steps, the coarser the picture. Consequently, the long-range interaction strength  $\beta'$  should decay with distance in a more realistic model, which indicates the decay of  $\beta'$  with respect to iteration steps in the RG framework. Even with this consideration, the overall picture presented above remains the same. In Eq. (7), if the interaction constant  $\beta'$  is decaying with the distance transient chaotic behavior could still be seen within some finite steps depending on the decaying rate. In Figs. 4(c) and 4(d), we plot the Julia sets for two decaying scenarios: (c) a power law decay  $\beta' \sim CP^{-\alpha}$  and (d) an exponential decay  $\beta' \sim Ce^{-P\alpha}$ , where  $C$  is a constant and  $P$  is the number of iteration steps.  $\alpha$  is a parameter used to control the decay rate.

In Figs. 4(c) and 4(d), we find that the Julia sets still meet the real axis at a finite interval. But this chaos is essentially transient since with  $P \rightarrow \infty$  the long-range interaction decays to zero and only one type of interaction remains, which restores the common ferro- or antiferromagnetic behavior. Nevertheless, if the decaying rate is small, the glass transition may still be observable in a finite-sized piece of bulk material.

### IV. THERMODYNAMICS ON THE HIERARCHICAL DIAMOND LATTICE

In the following, we calculate thermodynamic functions of the model to see how they are related to the Julia set based on the partition function [17]. In the previous computation, we took the lattice structure up to the 30th level where the number  $\gamma$  of spins in the model reaches  $2 + m(n-1)\left(\frac{(mn)^{29}-1}{mn-1}\right)$ . Expectedly, the extensive thermal quantity of the whole system will increase with  $\gamma$  linearly in the thermodynamic limit. From the free energy  $F = -k_B T \ln Z$ , we may compute the internal energy  $\langle E \rangle = -\frac{\partial}{\partial \beta} \ln Z$  and the entropy  $S = (\langle E \rangle - F)/T$ . Below, we evaluate the average values per spin of these quantities. For convenience, we take  $T = 1$ ,  $k_B = 1$ , and the calculation details are given in Appendix C. In Fig. 5(a), the average free energy is plotted in the interval  $[1, 3.5]$  at the parameters  $\lambda = 3$ ,  $m = 6$ ,  $n = 2$ , and  $\beta' = 2$ , which decreases when  $J$  increases, as expected in a ferromagnetic interaction. The average internal energy vs  $J$  is plotted in Fig. 5(b), which has a maximum at  $J \sim -1 = -\beta'/n$  indicating an antiferromagnetic interaction associated with the dashed lines in Fig. 1

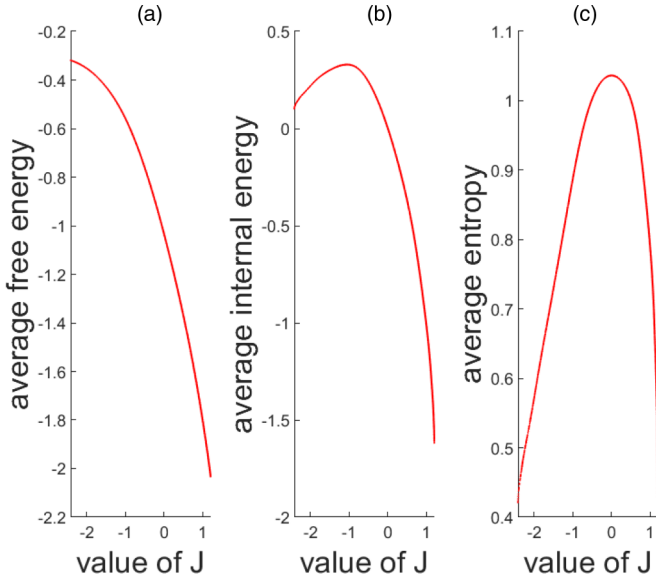


FIG. 5. Average free energy (a), the average internal energy (b), and the average entropy (c) vs  $J$  on the real axis for  $T = 1$ ,  $k_B = 1$ ,  $\lambda = 3$ ,  $m = 6$ ,  $n = 2$ , and  $\beta' = 2$ .

competing with the ferromagnetic one indicated by the solid lines. At  $J = 0$ , the entropy achieves its maximum value at  $J \approx 0$  as shown in Fig. 5(c), giving the maximum freedom to the points lying in the middle of a branch of the basic substituting unit.

## V. CONCLUSION

In this paper, we studied the chaotic dynamics of the RG transformation for the Potts model on diamond hierarchical lattices. By supplying long-range competing interactions to the original Potts model, chaos in the RG map becomes a common scene on the real axis. As a result, the Julia set, being identical to the set of Lee-Yang zeros in the thermodynamic limit, indeed meets the real axis at a closed interval. Unlike the previous case [24,38,46], here the number  $\lambda$  of spin states could assume a multitude of integer values and the interaction strength also seems reasonable, which may be physically more relevant [53]. Even in the chaotic regime, averages of thermodynamic functions are computed which look quite regular as the coupling constant changes in contrast to the irregular variation of the renormalized interaction strength.

The jump of the RG parameter indicates that at different scales the system may exhibit qualitatively different statistical behavior, which is a character of spin glass [30]. The added long-range interaction is antiferromagnetic in our model, which is competing with the original ferromagnetic interaction and hence possibly leads to the chaotic behavior of the effective interaction strength. This type of competition is also essential in spin glass, which leads to disorder and frustration. The current viewpoint is further strengthened by the observation that the emergence of chaos critically depends on the number  $n$  of bonds in each branch of the basic substituting unit. The competition is present and thus chaos chips in only when  $n$  is even. For an odd  $n$ , the RG map always settles to

a fixed point since the frustration could be mitigated in this configuration.

From the above analysis, chaos in the RG map arises due to the competition of interactions. Therefore, even though our computation was carried out to the Potts model on a hierarchical lattice which seems quite artificial, by introducing appropriate long-range interactions, we believe similar behavior should be observed in more general systems, e.g., a complex network with properly set parameter values. However, unlike the current case where the RG map could be derived exactly, it is still a challenge to extend the RG computation in this article to systems such as Potts model on scale-free or small-world networks [54].

## ACKNOWLEDGMENTS

This work was supported by the National Natural Science Foundation of China under Grants No. 11775035 and No. 12071047, the National Key R&D Program of China under Grant No. 2019YFB1406500, and also by the Fundamental Research Funds for the Central Universities with Contract No. 2019XD-A10.

## APPENDIX A: PROOF OF EQ. (4) AND EQ. (3)

From Sec. II, we know that the partition function of level  $N$  of our hierarchical diamond lattice can be written as

$$Z_N = \sum_{S_N} \exp \left[ \sum_{BD} [K\delta(s_i, s_j)] \right], \quad (\text{A1})$$

where  $\sum_{S_N}$  indicates a summation over states of all spins at level  $N$  and  $\sum_{BD}$  sums up all the spin pairs connected by a bond.

The RG transformation makes a local summation over the basic units so that the graph at level  $N$  reduces to the graph at level  $N - 1$ . Explicitly, we sum all the spins on each diamond block at the level  $N$  except the spins at end points connected by the edges at the level  $N - 1$ , and eliminate the spin variables in the partition function, so that the partition function formula at the level  $N$  can be expressed with the partition function at the level  $N - 1$ . First, we carry out the basic RG step reducing a diamond block to a bond. We use  $s_1$  and  $s_{n+1}$  to denote the states of two spins at two end points connected by the resulting bond after the reduction.

It is known that each diamond block is composed of  $m$  branches, each of which has  $n$  bonds. The new parameter  $K_1$  is used to denote the interaction strength after the RG transformation and  $K_2$  for the factor integrated out. The two spins  $s_1, s_{n+1}$  stand at the ends of all branches. The partition function of the diamond block could be written as

$$\begin{aligned} Z_{DBKRG} &= \sum_{S_{BD}} \prod_{BH} \sum_{NS_{BH}} \exp \left[ \sum_{BD} K\delta(s_i, s_j) \right] \\ &= \sum_{S_{BD}} \exp [K_1\delta(s_1, s_{n+1}) + K_2], \end{aligned} \quad (\text{A2})$$

where  $S_{BD}$  denotes the spin states of  $s_1, s_{n+1}$ ,  $BH$  for different branches, and  $NS_{BH}$  for the states of the  $n - 1$  spins between the end points on each branch. Because there is no interaction

between different branches except at  $s_1, s_{n+1}$ , we can sum the local spins on each branch independently and the resulting partition function of each branch is the same. Thus

$$Z_{DBKRG} = \sum_{S_{BD}} \left( \sum_{NS_{BH}} \exp \left[ K \sum_{BD} \delta(s_i, s_j) \right] \right)^m. \quad (A3)$$

Next, we carry out the summation  $\sum_{NS_{BH}}$  to decimate the  $n - 1$  intermediate spins on a branch. The resulting interaction strength  $K_{1_{BD}}$  and the factor  $K_{2_{BD}}$  are used in the branch partition function  $Z_{BH}$  after the RG decimation

$$Z_{BH}(K_{1_{BD}}, K_{2_{BD}}) = \sum_{s_1, s_{n+1}} \exp [K_{1_{BD}} \delta(s_1, s_{n+1}) + K_{2_{BD}}]. \quad (A4)$$

Two different cases are distinguished for the summation.

(i) When  $s_1 = s_{n+1}$ , after the RG transformation, the partition function is

$$Z_{BH}(K_{1_{BD}}, K_{2_{BD}}) = \lambda \exp (K_{1_{BD}} + K_{2_{BD}}), \quad (A5)$$

$$D = \begin{pmatrix} e^K - q - 1 & 0 & 0 & \dots & 0 & 1 \\ 0 & e^K - q - 1 & 0 & \dots & 0 & 2 \\ 0 & 0 & \dots & \dots & 0 & 3 \\ \dots & \dots & \dots & \dots & \dots & \dots \\ 0 & 0 & \dots & \dots & e^K - q - 1 & \lambda - 1 \\ 0 & 0 & \dots & \dots & 0 & e^K - q + \lambda - 1 \end{pmatrix}, \quad (A7)$$

from which we may find  $\lambda - 1$  identical eigenvalues  $e^K - 1$  and one singlet  $e^K + \lambda - 1$ . Thus

$$Z_{BH} = (e^K + \lambda - 1)^n + (\lambda - 1)(e^K - 1)^n. \quad (A8)$$

So

$$e^{K_{1_{BD}} + K_{2_{BD}}} = \frac{(e^K + \lambda - 1)^n + (\lambda - 1)(e^K - 1)^n}{\lambda}. \quad (A9)$$

(ii) When  $s_1 \neq s_{n+1}$ , the partition function after RG transformation is written as

$$Z_{BH}(K_{1_{BD}}, K_{2_{BD}}) = (\lambda^2 - \lambda)e^{K_{2_{BD}}}. \quad (A10)$$

To continue using the transfer matrix technique, one extra spin  $s_{n+2}$  may be added to connect with the spin  $s_{n+1}$  and assume that  $s_{n+2} = s_1$ . If there was no restriction on  $s_1$  and  $s_{n+1}$ , we have

$$\begin{aligned} Z_{BH1} &= (e^K + \lambda - 1)^{n+1} + (\lambda - 1)(e^K - 1)^{n+1} \\ &= (e^K + \lambda - 1)(e^K + \lambda - 1)^n \\ &\quad + (e^K - 1)(\lambda - 1)(e^K - 1)^n. \end{aligned} \quad (A11)$$

If the restriction  $s_1 = s_{n+1}$  is imposed, we have

$$Z_{BH1} = e^K (e^K + \lambda - 1)^n + e^K (\lambda - 1)(e^K - 1)^n. \quad (A12)$$

where  $\lambda$  is the number of states for each spin. A transfer matrix  $V$  could be used to do the summation  $Z_{BH} = TrV^n$ , where  $n$  is the number of bonds on the branch. The transfer matrix  $V$  is

$$V = \begin{pmatrix} e^K & 1 & 1 & \dots & 1 & 1 \\ 1 & e^K & 1 & \dots & 1 & 1 \\ 1 & 1 & e^K & \dots & 1 & 1 \\ \dots & \dots & \dots & e^K & \dots & 1 \\ 1 & 1 & \dots & \dots & e^K & 1 \\ 1 & 1 & \dots & \dots & 1 & e^K \end{pmatrix}. \quad (A6)$$

To get the trace, we need to solve the characteristic equations  $D = \|V - qE\| = 0$  to find all the eigenvalues [55]. Subtract the second column from the first one, the third column from the second, and so on. Then add the first row to the second one, the second row to the third, and so on. The matrix becomes very simple:

Therefore, the case with  $s_1 \neq s_{n+1}$  is obtained by subtracting Eq. (A12) from Eq. (A11),

$$Z_{BH} = (\lambda - 1)(e^K + \lambda - 1)^n + (-1)(\lambda - 1)(e^K - 1)^n, \quad (A13)$$

which results in

$$e^{K_{2_{BD}}} = \frac{(e^K + \lambda - 1)^n - (e^K - 1)^n}{\lambda} \quad (A14)$$

and thus

$$e^{K_{1_{BD}}} = \left[ \frac{(z + \lambda - 1)^n + (\lambda - 1)(z - 1)^n}{(z + \lambda - 1)^n - (z - 1)^n} \right], \quad (A15)$$

with regard to Eq. (A9). Considering all the  $m$  branches, we have

$$e^{K_2} = \left[ \frac{(e^K + \lambda - 1)^n - (e^K - 1)^n}{\lambda} \right]^m \quad (A16)$$

and

$$e^{K_1} = \left[ \frac{(e^K + \lambda - 1)^n + (\lambda - 1)(e^K - 1)^n}{(e^K + \lambda - 1)^n - (e^K - 1)^n} \right]^m. \quad (A17)$$

By replacing every diamond block with just one bond, we relate the partition function at level  $N$  to that at level  $N - 1$ ,

$$\begin{aligned} Z_N(K) &= \sum_{S_N} \exp \left[ \sum_{BD_N} [K \delta(s_i, s_j)] \right] \\ &= \sum_{S_{N-1}} \exp \left\{ \sum_{BD_{N-1}} [K_1 \delta(s_i, s_j)] + \sum_{BD_{N-1}} K_2 \right\} \end{aligned}$$

$$\begin{aligned}
&= \sum_{S_{N-1}} \left( \exp \left[ \sum_{BD_{N-1}} K_2 \right] \exp \left\{ \sum_{BD_{N-1}} [K_1 \delta(s_i, s_j)] \right\} \right) \\
&= \exp \left[ \sum_{BD_{N-1}} K_2 \right] \sum_{BD_{N-1}} \exp \left\{ \sum_{S_{N-1}} [K_1 \delta(s_i, s_j)] \right\} \\
&= \exp \left[ \sum_{BD_{N-1}} K_2 \right] Z_{N-1}(K_1), \tag{A18}
\end{aligned}$$

where  $BD_N, BD_{N-1}$  distinguishes the summation over all bonds at level  $N$  or level  $N-1$ . The summation of  $K_2$  is independent of spin variables so that it can be taken out. As  $(mn)^{N-2}$  bonds are present in the level  $N-1$ , we have

$$\exp \left( \sum_{BD} K_2 \right) = \exp [K_2 (mn)^{N-2}]. \tag{A19}$$

Thus

$$Z_N(K) = \exp [(mn)^{N-2} K_2] Z_{N-1}(K_1). \tag{A20}$$

If we denote  $e^{K_1} = \omega$ ,  $e^K = z$ , from Eq. (A20), Eq. (A16), and Eq. (A17), we get

$$Z_N(z) = \left[ \frac{(z + \lambda - 1)^n - (z - 1)^n}{\lambda} \right]^{m^{N-1} n^{N-2}} Z_{N-1}(\omega), \tag{A21}$$

where

$$\omega = U_{mn\lambda}(z) = \left[ \frac{(z + \lambda - 1)^n + (\lambda - 1)(z - 1)^n}{(z + \lambda - 1)^n - (z - 1)^n} \right]^m. \tag{A22}$$

## APPENDIX B: PROOF OF EQ. (7)

With the new hierarchical diamond lattice in Sec. III, if the strength of the long-range interaction is assumed to be  $-\beta'$ , we get

$$Z_N(K, \beta') = \sum_{S_N} \exp \left[ \sum_{BD} [K \delta(s_i, s_j)] + \sum_{S_{LRI}} (-\beta') \delta(s_i, s_j) \right], \tag{B1}$$

where  $S_{LRI}$  denotes the set of long-range interaction bonds. A similar process will be employed for an RG reduction to what has been done in the above section. In the calculation of the partition function of a branch, when  $s_1 = s_{n+1}$ , we still have

$$Z_{BH}(K_{1BD}, K_{2BD}) = \lambda \exp(K_{1BD} + K_{2BD}). \tag{B2}$$

In this case, the long range gives a factor  $e^{-\beta'}$  and thus

$$Z_{BH} = e^{-\beta'} [(e^K + \lambda - 1)^n + (\lambda - 1)(e^K - 1)^n], \tag{B3}$$

which results in

$$e^{K_{1BD} + K_{2BD}} = e^{-\beta'} \left[ \frac{(e^K + \lambda - 1)^n + (\lambda - 1)(e^K - 1)^n}{\lambda} \right]. \tag{B4}$$

When the  $s_1 \neq s_{n+1}$ , the long-range interaction does not contribute and so we get the same expression as before:

$$e^{K_{2BD}} = \frac{(e^K + \lambda - 1)^n - (e^K - 1)^n}{\lambda}. \tag{B5}$$

Denoting  $e^K = z$ , from Eqs. (B4) and (B5), we get

$$e^{K_{1BD}} = e^{-\beta'} \left[ \frac{(z + \lambda - 1)^n + (\lambda - 1)(z - 1)^n}{(z + \lambda - 1)^n - (z - 1)^n} \right]. \tag{B6}$$

In a diamond block with  $m$  branches, there is only one dashed line. Hence

$$e^{K_1} = e^{-\beta'} \left[ \frac{(z + \lambda - 1)^n + (\lambda - 1)(z - 1)^n}{(z + \lambda - 1)^n - (z - 1)^n} \right]^m \tag{B7}$$

and

$$e^{K_2} = \left[ \frac{(z + \lambda - 1)^n - (z - 1)^n}{\lambda} \right]^m. \tag{B8}$$

In the RG reduction, the long-range interaction at the lower level does not change. In this function,  $f_{N-1}(\beta')$  is used to represent  $\exp\{\sum_{OLRI} [(-\beta')\delta(s_i, s_j)]\}$ , which represents the summation of the long-range interaction built before level  $N-1$ . Then we make  $e^{K_1} = \omega$ ,  $e^K = z$ . If we take the previous calculation of  $e^{K_1}$ ,  $e^{K_2}$  into the above function, we can get

$$Z_N(z, \beta') = \left[ \frac{(z + \lambda - 1)^n - (z - 1)^n}{\lambda} \right]^{m^{j-1} n^{j-2}} Z_{N-1}(\omega, \beta'), \tag{B9}$$

where

$$\begin{aligned}
\omega &= e^{k_1} = U_{mn\lambda\beta'}(z) \\
&= e^{-\beta'} \left[ \frac{(z + \lambda - 1)^n + (\lambda - 1)(z - 1)^n}{(z + \lambda - 1)^n - (z - 1)^n} \right]^m. \tag{B10}
\end{aligned}$$

From the above computation, it is easy to see that even if  $\beta'$  changes with level the renormalization is similar, which results in

$$\begin{aligned}
Z_N(z, \{\beta'_i\}_{i=2, \dots, N}) \\
&= \left[ \frac{(z + \lambda - 1)^n - (z - 1)^n}{\lambda} \right]^{m^{j-1} n^{j-2}} \\
&\quad \times Z_{N-1}(\omega, \{\beta'_i\}_{i=2, \dots, N-1}), \tag{B11}
\end{aligned}$$

where  $\beta'_i$  denote the interaction strength at the  $i$ th level and the RG map  $\omega$  is

$$\omega = U_{mn\lambda\beta'_N}(z) = e^{-\beta'_N} \left[ \frac{(z + \lambda - 1)^n + (\lambda - 1)(z - 1)^n}{(z + \lambda - 1)^n - (z - 1)^n} \right]^m. \tag{B12}$$

## APPENDIX C: CALCULATION PROCESS OF THERMODYNAMICS

From Eqs. (4) and (3), we get

$$Z_j(z) = f_{mn\lambda j}(z) Z_{j-1}(\omega), \tag{C1}$$

where

$$f_{mn\lambda j}(z) = \left[ \frac{(z + \lambda - 1)^n - (z - 1)^n}{\lambda} \right]^{m^{j-1} n^{j-2}}. \tag{C2}$$

For convenience, we write  $f_{mn\lambda j}(z)$  as  $f_j(z)$ . At the first level, the lattice is a line, so that we can directly calculate the partition function as  $Z_1(z) = \lambda(z + \lambda - 1)$ , which is the starting

point of the iteration Eq. (C1). The average free energy is then computed as

$$\begin{aligned}
 F &= -\gamma^{-1} k_B T \ln Z_j(z) \\
 &= -\gamma^{-1} k_B T \{\ln [Z_{j-1}(\omega_{j-1}) f_j(z)]\} \\
 &= -\gamma^{-1} k_B T \{\ln [Z_{j-1}(\omega_{j-1})] + \ln [f_j(z)]\} \\
 &= -\gamma^{-1} k_B T \{\ln [Z_{j-2}(\omega_{j-2}) f_{j-1}(\omega_{j-1})] + \ln [f_j(z)]\} \\
 &\dots \\
 &= -\gamma^{-1} k_B T \{\ln [Z_1(\omega_1)] + \ln [f_2(\omega_2)] + \dots \\
 &\quad + \ln [f_{j-1}(\omega_{j-1})] + \ln [f_j(z)]\}, \tag{C3}
 \end{aligned}$$

where  $\gamma$  is the total number of spins at level  $j$  and  $Z_i$  is the partition function at the  $i$ th level of the hierarchical lattice.  $\omega_{i-1} = U_{mnl}(\omega_i)$  with  $\omega_j = z$ . We may write  $k_B T = J / \ln(z)$  and if  $T = 1$ ,  $k_B = 1$  is taken for convenience,  $J = \ln(z)$ .

The internal energy could be computed as

$$\begin{aligned}
 \langle E \rangle &= -\gamma^{-1} \frac{\partial}{\partial \beta} \ln Z = -\gamma^{-1} \frac{\partial}{\partial \beta} \ln Z_j(z) \\
 &= -\gamma^{-1} \frac{\partial}{\partial \beta} \{\ln [Z_{j-1}(\omega_{j-1}) f_j(z)]\}
 \end{aligned}$$

$$\begin{aligned}
 &= -\gamma^{-1} \frac{\partial}{\partial \beta} \{\ln [Z_{j-1}(\omega_{j-1})] + \ln [f_j(z)]\} \\
 &= -\gamma^{-1} \frac{\partial}{\partial \beta} \{\ln [Z_{j-2}(\omega_{j-2}) f_{j-1}(\omega_{j-1})] + \ln [f_j(z)]\} \\
 &\dots \\
 &= -\gamma^{-1} \frac{\partial}{\partial \beta} \{\ln [Z_1(\omega_1)] + \ln [f_2(\omega_2)] \\
 &\quad + \ln [f_3(\omega_3)] \dots + \ln [f_j(z)]\}, \tag{C4}
 \end{aligned}$$

where  $\omega_2$  is a function of  $\omega_1$ ,  $\omega_3$  is a function of  $\omega_2 \dots$ , and  $\omega_{j-1}$  is a function of  $z$ . When taking the derivative with respect to  $\beta$ , we need to use the chain rule

$$\begin{aligned}
 \langle E \rangle &= -\gamma^{-1} \frac{\partial z}{\partial \beta} \left\{ \frac{\partial \omega_{j-1}}{\partial z} \dots \frac{\partial \omega_2}{\partial \omega_3} \frac{\partial \omega_1}{\partial \omega_2} \frac{\partial}{\partial \omega_1} \ln [Z_1(\omega_1)] \right. \\
 &\quad \left. + \frac{\partial \omega_{j-1}}{\partial z} \dots \frac{\partial \omega_3}{\partial \omega_4} \frac{\partial \omega_2}{\partial \omega_3} \frac{\partial}{\partial \omega_2} \ln [f_2(\omega_2)] \right. \\
 &\quad \left. \dots + \frac{\partial}{\partial z} \ln [f_j(z)] \right\}. \tag{C5}
 \end{aligned}$$

- 
- [1] C. N. Yang and T. D. Lee, *Phys. Rev.* **87**, 404 (1952).  
[2] T. D. Lee and C. N. Yang, *Phys. Rev.* **87**, 410 (1952).  
[3] K. Huang, *Statistical Mechanics*, 2nd ed. (Wiley Press, New York, 1987).  
[4] M. Biskup, C. Borgs, J. T. Chayes, L. J. Kleinwaks, and R. Kotecky, *Phys. Rev. Lett.* **84**, 4794 (2000).  
[5] M. E. Fisher, *Rev. Mod. Phys.* **46**, 597 (1974).  
[6] A. A. Migdal, *Sov. Phys. JETP* **42**, 743 (1975).  
[7] A. N. Berker and S. Ostlund, *J. Phys. C: Solid State* **12**, 4961 (1979).  
[8] B. Derrida, L. D. Seze, and C. Itzykson, *J. Stat. Phys.* **33**, 559 (1983).  
[9] J. L. Cardy, *Phys. Rev. Lett.* **54**, 1354 (1985).  
[10] M. Kaufman and R. B. Griffiths, *J. Phys. A* **15**, L239 (1982).  
[11] B. Derrida, J.-P. Eckmann, and A. Erzan, *J. Phys. A* **16**, 893 (1983).  
[12] B. Derrida, C. Itzykson, and J. M. Luck, *Commun. Math. Phys.* **94**, 115 (1984).  
[13] B. Hu and B. Lin, *Phys. Rev. A* **39**, 4789 (1989).  
[14] P. M. Bleher and M. Y. Lyubich, *Commun. Math. Phys.* **141**, 453 (1991).  
[15] J. Stephenson, *Physica A* **136**, 160 (1989).  
[16] S.-Y. Kim, *Phys. Rev. Lett.* **93**, 130604 (2004).  
[17] R. K. Pathria, *Statistical Mechanics* (Butterworth-Heinemann Press, London, 1972).  
[18] T. L. Curtright, X. Jin, and C. K. Zachos, *Phys. Rev. Lett.* **108**, 131601 (2012).  
[19] S. Bachmann and B. Nachtergaele, *J. Stat. Phys.* **154**, 91 (2014).  
[20] M. Nife and H. J. Hilhorst, *Phys. Rev. Lett.* **68**, 2992 (1992).  
[21] B. P. Dolan and D. A. Johnston, *Phys. Rev. E* **65**, 057103 (2002).  
[22] E. Ilker and A. N. Berker, *Phys. Rev. E* **87**, 032124 (2013).  
[23] E. Ilker and A. N. Berker, *Phys. Rev. E* **89**, 042139 (2014).  
[24] S. R. McKay, A. N. Berker, and S. Kirkpatrick, *Phys. Rev. Lett.* **48**, 767 (1982).  
[25] A. N. Berker and S. R. McKay, *J. Stat. Phys.* **36**, 787 (1984).  
[26] A. J. Bray and M. A. Moore, *Phys. Rev. Lett.* **58**, 57 (1987).  
[27] T. Jörg and F. Krzakala, *J. Stat. Mech.: Theory Exp.* (2012) L01001.  
[28] T. K. Kopeć and M. Bogdan, *Phys. Lett. A* **377**, 2581 (2013).  
[29] G. Toulouse, Theory of the frustration effect in spin glasses: I, in *Spin Glass Theory and Beyond: An Introduction to the Replica Method and its Applications*, edited by M. Mezard *et al.* (World Scientific Press, Singapore, 1986), pp. 99–103.  
[30] K. Binder and A. P. Young, *Disordered and Frustrated Spin Systems* (John Wiley and Sons Press, New York, 2007).  
[31] S. F. Edwards and P. W. Andersen, *J. Phys. F* **5**, 965 (1975).  
[32] R. B. Griffiths and M. Kaufman, *Phys. Rev. B* **26**, 5022 (1982).  
[33] P. H. Damgaard and G. Thorleifsson, *Phys. Rev. A* **44**, 2738 (1991).  
[34] B. P. Dolan, *Phys. Rev. E* **52**, 4512 (1995).  
[35] Y. Matsuda, M. Müller, H. Nishimori, T. Obuchi, and A. Scardicchio, *J. Phys. A* **43**, 285002 (2010).  
[36] A. Türkoğlu and A. N. Berker, *Phys. Rev. E* **102**, 022122 (2020).  
[37] A. N. Berker and L. P. Kadanoff, *J. Phys. A* **13**, L259 (1980).  
[38] J. Qiao, *Mem. Am. Math. Soc.* **234**, 1 (2014).  
[39] J. Qiao, *Sci. China Ser. A* **48**, 388 (2005).  
[40] Y. Jiang, *Renormalization and Geometry in One-Dimensional and Complex Dynamics* (World Scientific Press, Singapore, 1996).  
[41] A. Raju, C. B. Clement, L. X. Hayden, J. P. Kent-Dobias, D. B. Liarte, D. Z. Rocklin, and J. P. Sethna, *Phys. Rev. X* **9**, 021014 (2019).  
[42] J. Qiao, *Sci. China Ser. A* **46**, 415 (2003).  
[43] S.-C. Chang, R. K. W. Roeder, and R. Shrock, *J. Math. Phys.* **61**, 073301 (2020).  
[44] A. Erzan, *Phys. Lett. A* **93**, 237 (1983).  
[45] F. Y. Wu, *Rev. Mod. Phys.* **54**, 235 (1982).

- [46] N. M. Svrakic, J. Kertesz, and W. Selke, *J. Phys. A* **15**, L427 (1982).
- [47] S. H. Strogatz, *Nonlinear Dynamics and Chaos* (Westview Press, Boulder, CO, 1994).
- [48] K. Binder and A. P. Young, *Rev. Mod. Phys.* **58**, 801 (1986).
- [49] F. Ritort, *Phys. Rev. B* **50**, 6844 (1994).
- [50] M. Sasaki, K. Hukushima, H. Yoshino, and H. Takayama, *Phys. Rev. Lett.* **95**, 267203 (2005).
- [51] B. Derrida, *Physica D* **107**, 186 (1997).
- [52] W.-K. Chen, *Ann. Probab.* **41**, 3345 (2013).
- [53] X. Peng, H. Zhou, B.-B. Wei, J. Cui, J. Du, and R.-B. Liu, *Phys. Rev. Lett.* **114**, 010601 (2015).
- [54] A.-L. Barabasi, *Science* **325**, 412 (2009).
- [55] G. Mussardo, *Statistical Field Theory: An Introduction to Exactly Solved Models in Statistical Physics* (Oxford University Press, Oxford, 2010).